

AD-A172 588

THE EFFECT OF BEAM QUALITY ON THE FREE-ELECTRON LASER
(U) NAVAL RESEARCH LAB WASHINGTON DC H P FREUND ET AL.
29 AUG 86 NRL-MR-5778

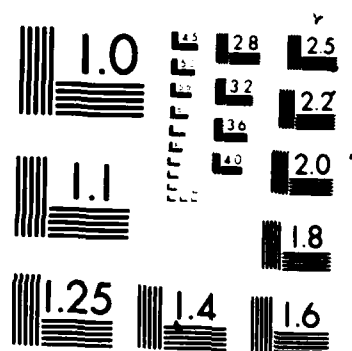
1/1

UNCLASSIFIED

F/G 28/5

NL





MICROCOPY RESOLUTION TEST CHART
NATIONAL BUREAU OF STANDARDS 1963-A

The Effect of Beam Quality on the Free-Electron Laser

H. P. FREUND* AND A. K. GANGULY

**Science Applications International Corp.
McLean, VA 22102*

*Microwave & Millimeter Wave Tube Technology Branch
Electronics Technology Division*

AD-A172 580

DTIC
ELECTE
OCT 06 1986
S D

FILE COPY

Approved for public release; distribution unlimited.

86 10 3 005

SECURITY CLASSIFICATION OF THIS PAGE

AD-A171580

REPORT DOCUMENTATION PAGE

1a. REPORT SECURITY CLASSIFICATION UNCLASSIFIED			1b. RESTRICTIVE MARKINGS		
2a. SECURITY CLASSIFICATION AUTHORITY			3. DISTRIBUTION/AVAILABILITY OF REPORT		
2b. DECLASSIFICATION/DOWNGRADING SCHEDULE			Approved for public releas, distribution unlimited.		
4. PERFORMING ORGANIZATION REPORT NUMBER(S) NRL Memorandum Report 5770			5. MONITORING ORGANIZATION REPORT NUMBER(S)		
6a. NAME OF PERFORMING ORGANIZATION Naval Research Laboratory		6b. OFFICE SYMBOL (if applicable) 6840	7a. NAME OF MONITORING ORGANIZATION		
6c. ADDRESS (City, State, and ZIP Code) Washington, DC 20375-5000			7b. ADDRESS (City, State, and ZIP Code)		
8a. NAME OF FUNDING/SPONSORING ORGANIZATION Office of Naval Research		8b. OFFICE SYMBOL (if applicable) 6841	9. PROCUREMENT INSTRUMENT IDENTIFICATION NUMBER		
8c. ADDRESS (City, State, and ZIP Code) Arlington, VA 22217			10. SOURCE OF FUNDING NUMBERS		
PROGRAM ELEMENT NO. 61153N		PROJECT NO. 68-0755-06	TASK NO. RR-021 -03-46	WORK UNIT ACCESSION NO. DN980-028	
11. TITLE (Include Security Classification) The Effect of Beam Quality on the Free-Electron Laser					
12. PERSONAL AUTHOR(S) Freund H.P., and Ganguly A.K.					
13a. TYPE OF REPORT NRL Memo Report		13b. TIME COVERED FROM TO		14. DATE OF REPORT (Year, Month, Day) 1986 August 29	
15. PAGE COUNT 16					
16. SUPPLEMENTARY NOTATION *Science Applications International Corp., McLean, VA 22102					
17. COSATI CODES			18. SUBJECT TERMS (Continue on reverse if necessary and identify by block number)		
FIELD	GROUP	SUB-GROUP	Free-Electron laser		
			Coherent sources of radiation		
19. ABSTRACT (Continue on reverse if necessary and identify by block number)					
<p>The effect of finite momentum spread on the Free-Electron Laser amplifier is investigated for a configuration of a helical wiggler and an axial guide magnetic field. A set of coupled nonlinear differential equations in three-dimensions describing the evolution of the electron trajectories and the radiation field is derived and solved numerically for several sets of parameters. The initial beam distribution is defined external to the wiggler field and the adiabatic injection of the beam into the wiggler is modeled by allowing the wiggler amplitude to increase slowly from zero to a constant amplitude over several wiggler periods. While the efficiency is found to decrease rapidly with increasing momentum spread, resonant effects between the wiggler and guide magnetic fields are found to substantially decrease the sensitivity of the saturation efficiency to the beam emittance. In addition, a relatively sharp change in the slope of the efficiency versus beam momentum spread is identified with the transition between the "cold" and "thermal" beam regimes.</p>					
20. DISTRIBUTION/AVAILABILITY OF ABSTRACT <input type="checkbox"/> UNCLASSIFIED/UNLIMITED <input checked="" type="checkbox"/> SAME AS RPT. <input type="checkbox"/> DTIC USERS			21. ABSTRACT SECURITY CLASSIFICATION UNCLASSIFIED		
22a. NAME OF RESPONSIBLE INDIVIDUAL A.K. Ganguly			22b. TELEPHONE (Include Area Code) (202) 767-3382		22c. OFFICE SYMBOL 6841

DD FORM 1473, 84 MAR

83 APR edition may be used until exhausted
All other editions are obsolete.

SECURITY CLASSIFICATION OF THIS PAGE

CONTENTS

I. INTRODUCTION	1
II. THE GENERAL EQUATIONS	2
III. NUMERICAL SIMULATION	5
IV. SUMMARY AND CONCLUSION	7
ACKNOWLEDGMENTS	8
REFERENCES	8



Accession For	
NTIS CRA&I	<input checked="" type="checkbox"/>
DTIC TAB	<input type="checkbox"/>
Unannounced	<input type="checkbox"/>
Justification	
By	
Distribution/	
Availability Codes	
Dist	Avail and/or Special
A-1	

THE EFFECT OF BEAM QUALITY ON THE FREE-ELECTRON LASER

I. INTRODUCTION

One of the most important current problems involved in the design and operation of the Free-Electron Laser (FEL) is the effect of an initial thermal spread in the electron beam velocity distribution upon both the linear gain and nonlinear saturation efficiency of the interaction. The physical mechanism underlying the concept of the FEL is the axial bunching of an electron beam in the ponderomotive wave formed by the beating of radiation and wiggler fields, and maximum operational efficiencies are obtained when saturation occurs by the trapping of the bulk of the electron beam in the ponderomotive potential. Such a process requires a highly coherent interaction involving both a narrow radiation spectrum and an extremely low axial velocity spread in the electron beam. Observe that a monoenergetic electron distribution is not sufficient to ensure operation in the trapped-particle regime, and the partition of energy between the axial and transverse directions is important.

The motivation of the present work is to develop a fully three-dimensional nonlinear formulation of the FEL amplifier for a configuration which consists of an electron beam propagating through a loss-free cylindrical waveguide in the presence of a helically symmetric wiggler and uniform axial guide magnetic field. The analysis we employ is an extension of previously described nonlinear analysis^{1,2} which treated the problem in the absence of an initial beam velocity spread. The formulation involves the derivation and numerical solution of a set of coupled nonlinear differential equations which describe the self-consistent evolution of both the trajectories of an ensemble of electrons and the electromagnetic fields. Space-charge fields, however, are neglected and the analysis is restricted to the high-gain Compton (or "strong-pump") regime of operation. The adiabatic injection of the electron beam is modeled by allowing the wiggler field amplitude to increase slowly from zero to a constant level. The initial electron beam distribution (i.e., external to the wiggler field region) is assumed to be monoenergetic but of finite emittance.³ Since we include the presence of an axial guide magnetic field in the formulation, the concept of beam emittance is ambiguous

and can be defined in various ways. For convenience in this paper, however, we use the term merely to describe an electron beam which is characterized by an initial momentum spread in (p_\perp, p_z) that describes a ring distribution subject to the condition that $p_\perp^2 + p_z^2 = \text{constant}$. Such a distribution describes an electron beam with both a transverse and axial energy spread, and the magnitude of the spread provides a measure of the electron beam quality for FEL applications. The propagation of the beam through the adiabatic entry region of the wiggler, therefore, describes the self-consistent evolution of the initial distribution due to the effect of the wiggler field. It should be remarked that there is no fundamental difficulty in the inclusion of a spread in the total energy as well, and the formulation can be readily generalized to describe a spread in the total energy. This occurs, however, at the expense of the inclusion of a larger number of electrons in the numerical simulation.

The organization of the paper is as follows. The general equations are presented in Sec. II. The coupled particle and field equations are solved numerically, and the results are described in Sec. III for a variety of parameters in order to illustrate the effect of the momentum spread on the operational efficiency of the FEL amplifier. Finally, a summary and conclusion is given in Sec. V.

II. THE GENERAL EQUATIONS

The physical configuration we employ describes the propagation of an electron beam through a loss-free cylindrical waveguide in the presence of an axial guide field and a helical wiggler field. The analysis is three-dimensional and we represent the static magnetic fields in cylindrical coordinates as

$$\mathbf{B}_s(\mathbf{x}) = B_0 \hat{\mathbf{e}}_z + 2B_w(z) \left[I_1'(\lambda) \hat{\mathbf{e}}_r \cos \chi - \frac{1}{\lambda} I_1(\lambda) \hat{\mathbf{e}}_\theta \sin \chi + I_1(\lambda) \hat{\mathbf{e}}_z \sin \chi \right], \quad (1)$$

where B_0 and B_w represent the axial and wiggler field amplitudes, $\lambda \equiv k_w r$, $\chi \equiv \theta - k_w z$, $k_w \equiv 2\pi/\lambda_w$ (where λ_w is the wiggler period), and $I_n(\lambda)$ and $I_n'(\lambda)$ are the modified Bessel function and its derivative. In order to model the realistic injection of the electron beam, we allow the wiggler amplitude to increase adiabatically to a constant amplitude over N_w wiggler periods, and write

$$B_w(z) = \begin{cases} B_w \sin^2(k_w z / 4N_w) & , 0 \leq z \leq N_w \lambda_w \\ B_w & , z > N_w \lambda_w \end{cases} \quad (2)$$

Space-charge fields are neglected, and the boundary conditions of the radiation field at the waveguide wall are satisfied by expanding the vector potential in terms of the basis functions of the vacuum guide. We restrict the analysis to the TE modes and write

$$\delta A(\mathbf{x}, t) = \sum_{n=1}^{\infty} \delta A_{ln}(z) \left[\frac{l}{k_{ln} r} J_l'(k_{ln} r) \hat{e}_r \sin \alpha_l + J_l'(k_{ln} r) \hat{e}_\theta \cos \alpha_l \right], \quad (3)$$

where for frequency ω and wavenumber $k(z)$

$$\alpha_l \equiv \int_0^z dz' k(z') + l\theta - \omega t, \quad (4)$$

$k_{ln} \equiv x'_{ln}/R_g$ ($R_g \equiv$ waveguide radius) for $J_l'(x'_{ln}) = 0$, and $J_l(x)$ and $J_l'(x)$ are the regular Bessel function of the first kind and its derivative. Both the mode amplitude $\delta A_{ln}(z)$ and the wavevector $k(z)$ are assumed to vary slowly over a wave period. The electron beam is assumed to be initially (i.e., at $z = 0$) monoenergetic, but with a momentum distribution in the form of a "ring" in the initial p_{10} and p_{z0} as follows:

$$F_0(\mathbf{p}_0) = A \exp(-(p_{z0} - p_0)^2/\Delta p_z^2) \delta(p_0^2 - p_{10}^2 - p_{z0}^2) \Theta(p_{z0}) \quad (5)$$

where $(p_0, \Delta p_z)$ represent the total momentum and axial momentum spread of the beam, $\Theta(x)$ is the Heaviside function, and the normalization constant is

$$A = \left(\pi \int_0^{p_0} dp_{z0} \exp(-(p_{z0} - p_0)^2/\Delta p_z^2) \right)^{-1}. \quad (6)$$

Note, therefore, that Δp_z describes a spread in both axial and transverse momenta.

The derivation of the equations governing the evolution of $\delta A_{ln}(z)$ and $k(z)$ proceeds in the same manner described by Ganguly and Freund,^{1,2} and we find that

$$\frac{d^2}{dz^2} \delta a_{ln} + \left(\frac{\omega^2}{c^2} - k^2 - k_{ln}^2 \right) \delta a_{ln} = \frac{\omega_b^2}{c^2} \beta_{z0} H_{ln} < \frac{v_1 T_l^{(+)} + v_2 W_l^{(+)}}{|v_z|} >, \quad (7)$$

$$2k^{1/2} \frac{d}{dz} (k^{1/2} \delta a_{ln}) = \frac{\omega_b^2}{c^2} \beta_{z0} H_{ln} < \frac{v_1 W_l^{(-)} - v_2 T_l^{(-)}}{|v_z|} >, \quad (8)$$

where $\delta a_{ln} \equiv e \delta A_{ln} / mc^2$, $\beta_{z0} \equiv v_{z0}/c$, $\omega_b^2 \equiv 4\pi e^2 n_b / m$, (v_1, v_2) are the transverse components of the velocity relative to the basis vectors $\hat{e}_1 = \hat{e}_x \cos k_w z + \hat{e}_y \sin k_w z$, $\hat{e}_2 = -\hat{e}_x \sin k_w z + \hat{e}_y \cos k_w z$,

$$H_{ln} \equiv \frac{x_{ln}'^2}{(x_{ln}'^2 - l^2) J_l'^2(x_{ln}')}, \quad (9)$$

$T_l^{(\pm)} \equiv F_l^{(\pm)} \sin \psi_l + G_l^{(\pm)} \cos \psi_l$, and $W_l^{(\pm)} \equiv F_l^{(\mp)} \cos \psi_l - G_l^{(\mp)} \sin \psi_l$. In addition,

$$F_l^{(\pm)} \equiv J_{l-1}(k_{ln} r) \cos(l-1)\chi \pm J_{l+1}(k_{ln} r) \cos(l+1)\chi,$$

$$G_l^{(\pm)} \equiv J_{l-1}(k_{ln} r) \sin(l-1)\chi \pm J_{l+1}(k_{ln} r) \sin(l+1)\chi, \quad (10)$$

and

$$\psi_1 \equiv \psi_0 + \int_0^z dz' \left[k - ik_w - \frac{\omega}{v_z} \right] \quad (11)$$

is the particle phase relative to the ponderomotive wave ($\psi_0 = -\omega t_0$). These equations are formally identical to those derived previously, except that average operator ($A_g = \pi R_g^2$)

$$\begin{aligned} \langle (\dots) \rangle &\equiv \frac{A}{4\pi^2 R_g^2} \int_0^{2\pi} d\phi_0 \int_0^{p_0} dp_{z0} \frac{p_{z0}}{p_0} \exp(- (p_{z0} - p_0)^2 / \Delta p_z^2) \\ &\times \int_{-\pi}^{\pi} d\psi_0 \sigma_{||}(\psi_0) \int_{A_g} d\theta_0 dr_0 r_0 \sigma_{\perp}(r_0, \theta_0) (\dots) \end{aligned} \quad (12)$$

now includes the initial momentum space coordinates p_{z0} and $\phi_0 \equiv \tan^{-1}(p_{y0}/p_{x0})$. Note that $\sigma_{||}(\psi_0)$ and $\sigma_{\perp}(r_0, \theta_0)$ describe the initial electron distribution in phase and cross-section. For simplicity, we assume the beam to be uniformly distributed in phase ($\sigma_{||} = 1$) and cross-section for a given beam radius R_b (i.e., $\sigma_{\perp} = 1$ for $0 \leq r < R_b$).

Finally, in order to complete the formulation, the electron orbit equations must be specified by the Lorentz force equations. For the particular static and fluctuating fields described previously, we find that for the TE_n mode

$$\begin{aligned} v_z \frac{d}{dz} p_1 &= -\frac{1}{\gamma} [\Omega_0 - \gamma k_w v_z + 2\Omega_w I_1(\lambda) \sin \chi] p_2 + \frac{1}{\gamma} \Omega_w p_z I_2(\lambda) \sin 2\chi \\ &- \frac{1}{2} mc \delta a_n [(\omega - k v_z) W_l^{(-)} - 2k_{in} v_z J_l(k_{in} r) \cos \alpha_l \\ &- \Gamma_{in} v_z T_l^{(+)}], \end{aligned} \quad (13)$$

$$\begin{aligned} v_z \frac{d}{dz} p_2 &= \frac{1}{\gamma} [\Omega_0 - \gamma k_w v_z + 2\Omega_w I_1(\lambda) \sin \chi] p_1 \\ &- \frac{1}{\gamma} \Omega_w p_z [I_0(\lambda) + I_2(\lambda) \cos 2\chi] \\ &+ \frac{1}{2} mc \delta a_n [(\omega - k v_z) T_l^{(-)} - 2k_{in} v_z J_l(k_{in} r) \cos \alpha_l \\ &+ \Gamma_{in} v_z W_l^{(+)}], \end{aligned} \quad (14)$$

$$\begin{aligned} v_z \frac{d}{dz} p_z &= \frac{1}{\gamma} \Omega_w p_2 [I_0(\lambda) + I_2(\lambda) \cos 2\chi] - \frac{1}{\gamma} \Omega_w p_1 I_2(\lambda) \sin 2\chi \\ &- \frac{1}{2} mc \delta a_n [k(v_1 W_l^{(-)} - v_2 T_l^{(-)}) \\ &+ \Gamma_{in} (v_1 T_l^{(+)} + v_2 W_l^{(-)})] \end{aligned} \quad (15)$$

where $\Omega_{0,w} \equiv |eB_{0,w}/mc|$, $\gamma \equiv (1 - v^2/c^2)^{-1/2}$, and $\Gamma_{in} \equiv d(\ln \delta a_{in})/dz$. In addition,

$$v_z \frac{d}{dz} x = v_1 \cos k_w z - v_2 \sin k_w z, \quad (16)$$

$$v_z \frac{d}{dz} y = v_1 \sin k_w z + v_2 \cos k_w z, \quad (17)$$

and

$$\frac{d}{dz} \psi_1 = k + lk_w - \frac{\omega}{v_z}. \quad (18)$$

III. NUMERICAL SIMULATION

We first consider several cases corresponding to the low axial guide field regime for which $\Omega_0 < \gamma_0 k_w v_{11}$. Case 1 is that of a 35-GHz amplifier, and we assume that $B_0 = 1.3$ kG, $B_w = 2$ kG, $\lambda_w = 1.175$ cm, and $N_w = 10$. The electron beam is characterized by an energy of 250 keV, a current of 35 A, and an initial radius $R_b = 0.155$ cm. This case has been considered previously in the absence of an initial velocity spread¹, and a maximum efficiency $\eta_0 = 21.4\%$ was found for a frequency $\omega/ck_w = 1.3$ (33.2 GHz) in the TE_{11} mode ($R_s = 0.36626$ cm). The effect of an initial velocity spread is shown in Fig. 1, in which we plot the saturation efficiency versus $\Delta p_z/p_0$. The decrease in efficiency with Δp_z is quite rapid, and an order of magnitude decrease in η is found to occur as the velocity spread increases to $\Delta p_z/p_0 \sim 2\%$. In terms of an axial energy spread we write

$$\frac{\Delta \gamma_z}{\gamma_0} = 1 - \left[1 + 2\gamma_0^2 \beta_0^2 \frac{\Delta p_z}{p_0} \right]^{-1/2}, \quad (19)$$

where $\gamma_0 = (1 + p_0^2/m^2 c^2)^{1/2}$, and $\beta_0 = p_0/\gamma_0 mc$. Hence, this order of magnitude decrease in the efficiency corresponds to $\Delta \gamma_z/\gamma_0 \sim 2.6\%$.

As shown by the numerical results, the saturation efficiency is highly sensitive to the axial energy spread of the beam. Typically, the axial energy spread must be much less than the depth of the ponderomotive potential in order for the trapping mechanism to be effective. On the basis of perturbations about an idealized three-dimensional class of helical trajectories,⁴ we obtain an estimate of the effective ponderomotive "depth" of²

$$\frac{\Delta v_{||}}{v_{||}} = 4 \sqrt{\frac{c |v_w \Phi|}{\gamma_0 \gamma^2 v_{||}^2} \delta a_{in} J_1'(k_{in} r_0)} \quad (20)$$

where $(v_w, v_{||})$ are the transverse and axial velocity components of the helical orbits, $\gamma^2 = (1 - v^2/c^2)^{-1}$, r_0 is the radius of the orbit about the axis of symmetry, Φ is a complicated

function of the orbit parameters given in Ref. 2, and the normalized radiation amplitude $\delta a_{\parallel n}$ is to be evaluated at saturation (in the absence of thermal spread). Eq. (20) provides only a crude estimate of the trapping depth since the trajectories both in simulation and in actual experiments can differ from the helical orbits. However, if we relate $\Delta v_{\parallel}/v_{\parallel} \sim \Delta p_z/p_0$ and use Eq. (20) to obtain a measure of the effective ponderomotive energy spread $\Delta \gamma_{\text{pond}}/\gamma_0$, then we find that $\Delta \gamma_{\text{pond}}/\gamma_0 \sim 21\%$ for parameters associated with Case 1. This indicates that the efficiency has decreased by an order of magnitude as the axial energy spread approaches about 10% of the ponderomotive "trapping depth."

Case 2 corresponds to an FEL experiment at the Naval Research Laboratory^{5,6} which makes use of an electron beam with an energy of 750 keV, a current of 200 A, and an initial beam radius $R_b = 0.5$ cm. The experiment employs a helical wiggler with $B_w = 1$ kG, $\lambda_w = 4$ cm, and $N_w = 6$. No axial guide field is imposed. This case has also been studied previously,² and an efficiency of $\eta_0 \approx 7.27\%$ was found at a frequency $\omega/ck_w \approx 8.3$ (62.3 GHz) in the TE_{11} mode ($R_g = 1.5$ cm). The saturation efficiency is shown in Fig. 2 as a function of $\Delta p_z/p_0$, and it is evident that an order of magnitude decrease in the efficiency has occurred as the momentum spread increases to $\Delta p_z/p_0 \approx 0.21\%$. This corresponds to an axial energy spread of $\Delta \gamma_z/\gamma_0 \sim 1\%$. For this case, the ponderomotive trapping depth is $\Delta \gamma_{\text{pond}}/\gamma_0 \approx 15\%$ and, as for Case 1, the efficiency decreases by an order of magnitude as the axial energy spread approaches 10% of the "trapping depth." Finally, we interpret the relatively sharp transition of the scaling of η with Δp_z which occurs for $\Delta p_z/p_0 \sim 0.1$ -0.15 as due to the transition between the cold and thermal beam regimes. This will be discussed in more detail later in this section. We remark that such rapid declines in the efficiency with increasing momentum spread as shown in Cases 1 and 2 are consistent with results found previously by Kwan and Snell⁷ by means of a one-dimensional particle-in-cell simulation code.

In Case 3, we investigate the effect of a relatively small axial guide field on the scaling of the efficiency for parameters consistent with Case 2 by inclusion of a guide field of $B_g = 1$ kG. This is still far below the resonance condition for $\Omega_0 \sim \gamma_0 k_w v_{\parallel}$; however, the axial velocity is sufficiently reduced that the frequency regime over which gain occurs drops and we find an efficiency in the absence of a momentum spread $\eta_0 \approx 3.37\%$ at a frequency $\omega/ck_w \approx 7.5$ (56.2 GHz). The scaling of the efficiency versus $\Delta p_z/p_0$ for this case is shown in Fig. 3. It is clear from the figure that the effect of the guide field has been to reduce the sensitivity of the efficiency to the momentum spread since the efficiency has decreased by only about 80% relative to the zero momentum spread result for $\Delta p_z/p_0 \approx 0.6\%$. This contrasts with Case 2 in which an order of magnitude decrease in η was observed for $\Delta p_z/p_0 \approx 0.21\%$. We also note

that $\Delta p_z/p_0 \approx 0.6\%$ corresponds to an axial energy spread of $\Delta \gamma_z/\gamma_0 \approx 2.9\%$. Since $\Delta \gamma_{\text{pond}}/\gamma_0 \approx 19.1\%$ for this case, the 80% decrease in η corresponds to an axial energy spread of about 15% of the "trapping depth."

We now address the effect of a strong axial field on the sensitivity of the efficiency to the beam emittance. We observe that the effective ponderomotive energy spread (20) will increase as B_0 approaches the resonance at $\Omega_0 \sim \gamma_0 k_w v_{||}$, because v_w , Φ , and δA_{in}^2 are enhanced near the resonance while $v_{||}$ declines. Operation close to resonance, therefore, should result in a decreased sensitivity to beam emittance. In order to verify this conclusion numerically, we consider the effect of finite emittance in the regime in which $\Omega_0 \geq \gamma_0 k_w v_{||}$. The example (Case 4) of interest corresponds to the propagation of a 1 MeV, 50 A beam with $R_s = 0.2$ cm through a drift tube of radius 0.5 cm. The static magnetic fields are: $B_0 = 11.75$ kG, $B_w = 1.0$ kG, $\lambda_w = 3.0$ cm, and $N_w = 10$. This case exhibits a high efficiency and broad bandwidth in the zero momentum spread limit with a peak efficiency of $\eta_0 \approx 46.9\%$ at $\omega/c k_w = 3.0$ (30 GHz) in the TE_{11} mode.¹ The effect of finite emittance is shown in Fig. 4 in which we plot the normalized emittance versus $\Delta p_z/p_0$. Clearly, the efficiency decreases with emittance far more slowly than in either of the other cases, and decreases by an order of magnitude for $\Delta p_z/p_0 \approx 5-6\%$ (corresponding to $\Delta \gamma_z/\gamma_0 \sim 25\%$). As a result, we conclude that dramatic decreases in the sensitivity of the efficiency upon the initial beam emittance can be obtained from operation with strong axial fields close to the resonance at $\Omega_0 \geq \gamma_0 k_w v_{||}$.

Although the effect is more evident in Cases 2-4, all of the cases shown exhibit a relatively sudden change in the scaling of the efficiency versus $\Delta p_z/p_0$ which we attribute to the transition from the cold beam limit to the "thermal" regime in which the wave is resonant with only a small fraction of the electron beam due to finite momentum spread effects. An estimate of where this transition occurs may be obtained by noting that the cold beam limit occurs for $|Imk/Rek| \gg \Delta p_z/p_0$. We note that the ratio $|Imk/Rek| = 3.5\%$, 0.48% , 0.62% , and 1.8% for Cases 1-4 respectively. The determination of the precise range of the transition range between the cold and thermal regimes requires a detailed analysis of the linear dispersion properties of the modes in three-dimensions. However, we expect that this transition occurs for $\Delta p_z/p_0 \leq |Imk/Rek| \leq 3\Delta p_z/p_0$, which provides reasonable agreement with the numerical results.

IV. SUMMARY AND CONCLUSION

In this paper we have developed a three-dimensional nonlinear theory and simulation of the FEL amplifier in the high-gain Compton regime with the inclusion of a finite electron

beam momentum spread. The formulation describes the adiabatic injection of the electron-beam into the wiggler field region; hence the evolution of the beam distribution (initially defined external to the wiggler) as the beam enters the wiggler is described in a self-consistent manner. Results of the simulation indicate that in the low axial guide field regime the initial axial energy spread must be less than approximately 10% of the ponderomotive trapping depth at saturation (in the absence of momentum spread) in order for high efficiency operation to be achieved. However, the effect of the axial guide field appears to decrease the sensitivity of the efficiency to the momentum spread. This occurs due to the resonant enhancement of the ponderomotive trapping depth (20), and is most pronounced for high axial guide fields near the resonance at $\Omega_0 \lesssim \gamma_0 k_w v_{||}$. Finally, a relatively sharp transition in the scaling of the efficiency with the axial momentum spread is observed in simulation which is attributed to the transition from the cold beam to the "thermal" beam regime.

ACKNOWLEDGMENTS

This research was supported by the Office of Naval Research and the Office of Naval Technology. The authors would like to thank R.K. Parker, C.W. Roberson, P. Sprangle, C.M. Tang, and R.H. Jackson for helpful discussions.

REFERENCES

1. A.K. Ganguly and H.P. Freund, Phys. Rev. A32, 2275 (1985).
2. H.P. Freund and A.K. Ganguly, Phys. Rev. A33, 1060 (1986).
3. J.D. Lawson, *The Physics of Charged Particle Beams*, (Oxford University Press, Oxford, UK, 1977), Chap. 4.
4. P. Diament, Phys. Rev. A23, 2537 (1981).
5. J.A. Pasour, R.F. Lucey, and C.W. Roberson, in *Free-Electron Generators of Coherent Radiation*, eds. C.A. Brau, S.F. Jacobs, and M.O. Scully, Proc. SPIE 453 (1984), p. 328.
6. J.A. Pasour, R.F. Lucey, and C.A. Kapetanakis, Phys. Rev. Lett. 53, 1728 (1984).
7. T.J.T. Kwan and C.M. Snell, Phys. Fluids 26, 835 (1983).
8. H.P. Freund, Phys. Rev. A27, 1977 (1983).

TE₁₁ Mode ($R_g = 0.36626$ cm)

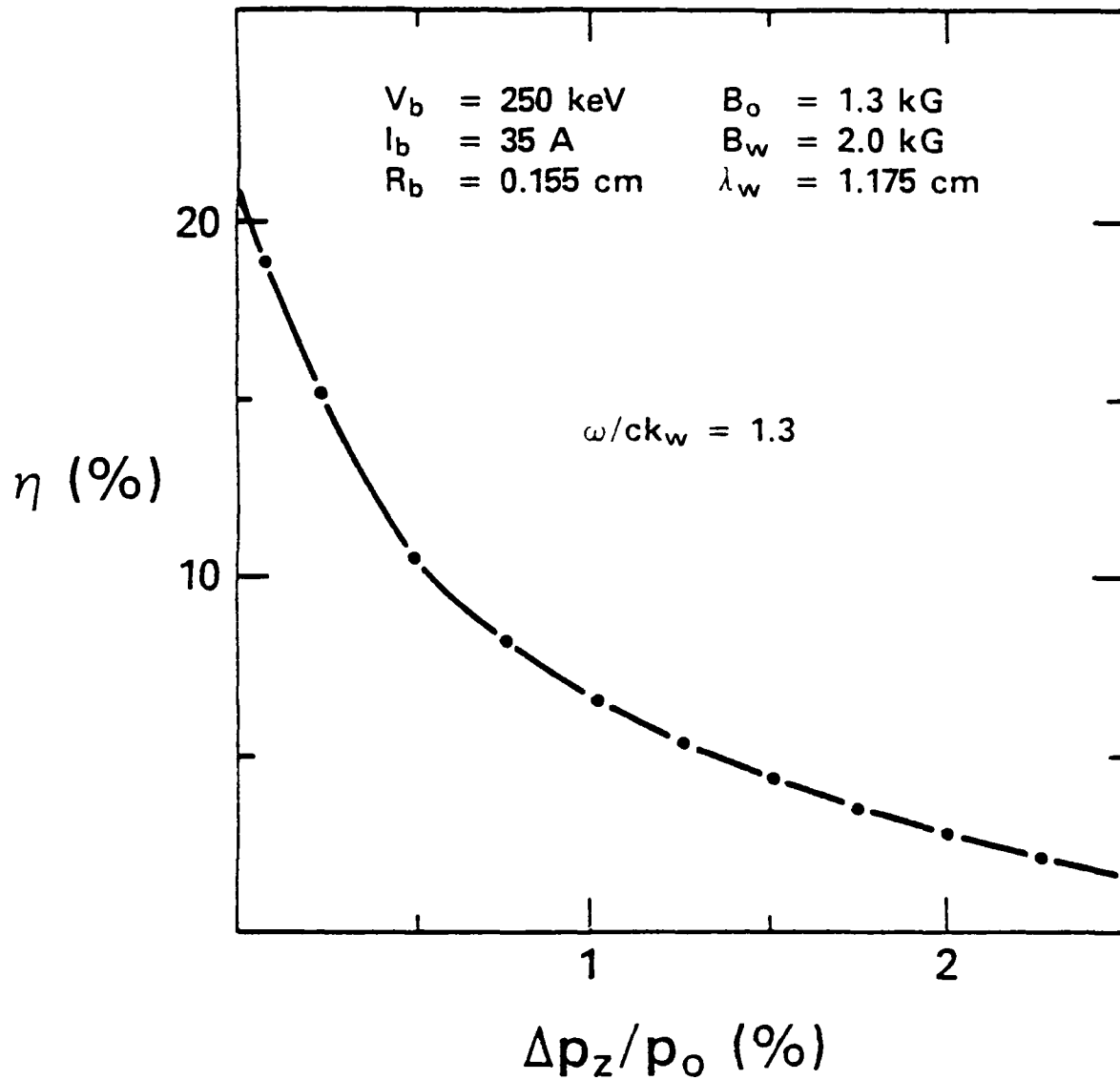


Fig. 1 — Graph of the efficiency versus axial momentum spread for Case 1

TE₁₁ Mode ($R_g = 1.5$ cm)

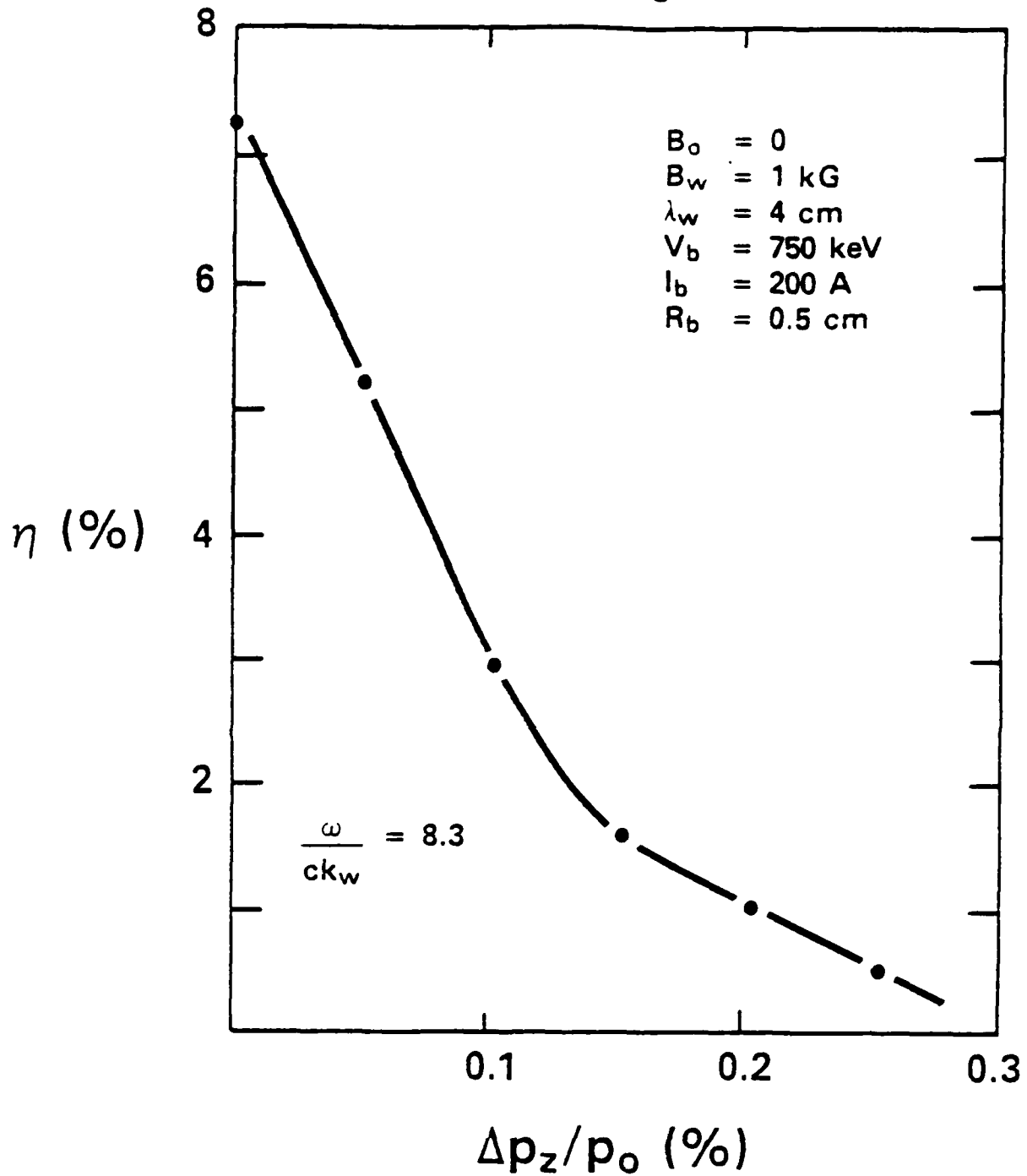


Fig. 2 — Graph of the efficiency versus axial momentum spread for Case 2

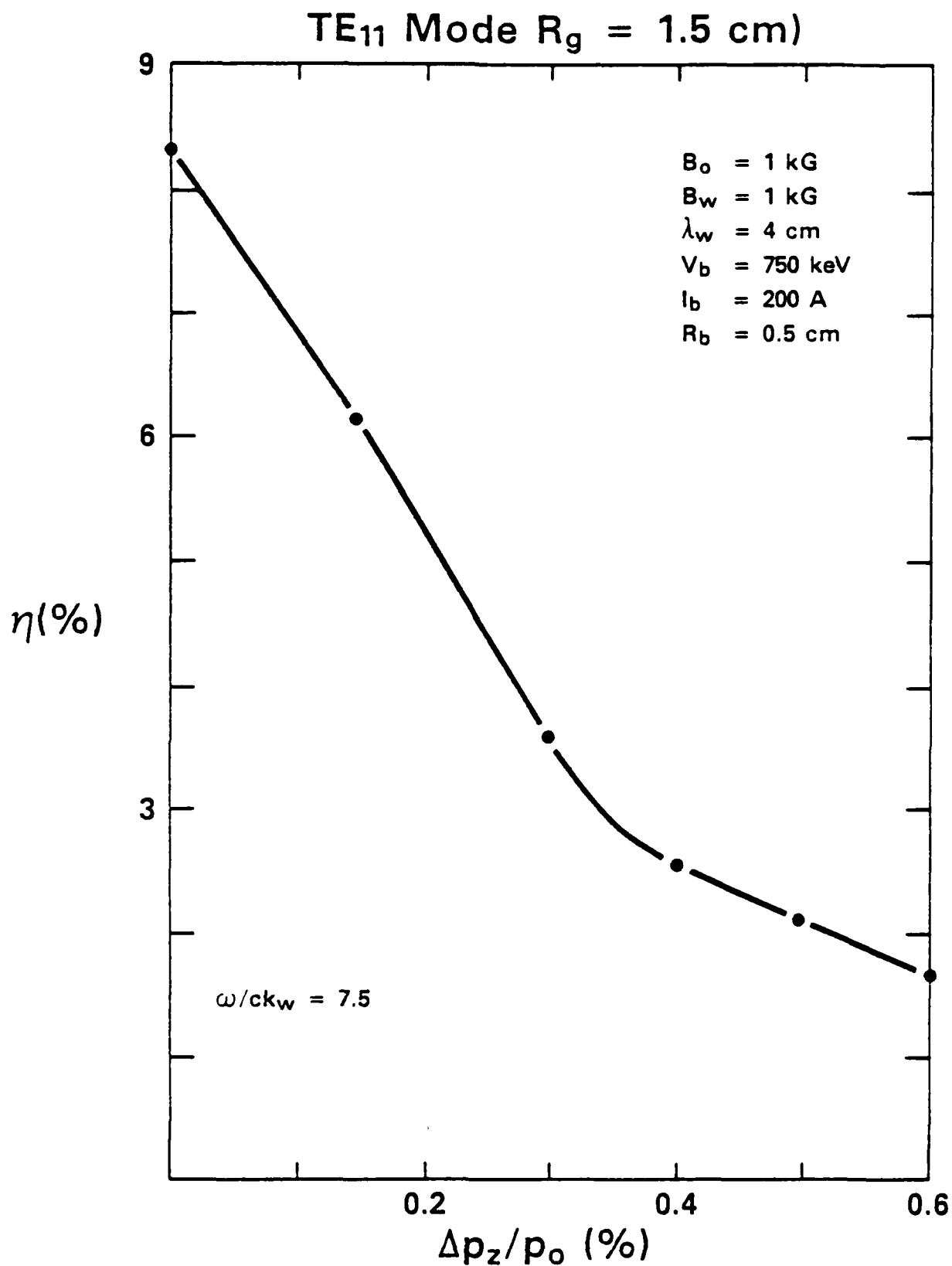


Fig. 3 — Graph of the efficiency versus axial momentum spread for Case 3

TE₁₁ Mode R_g = 0.5 cm)

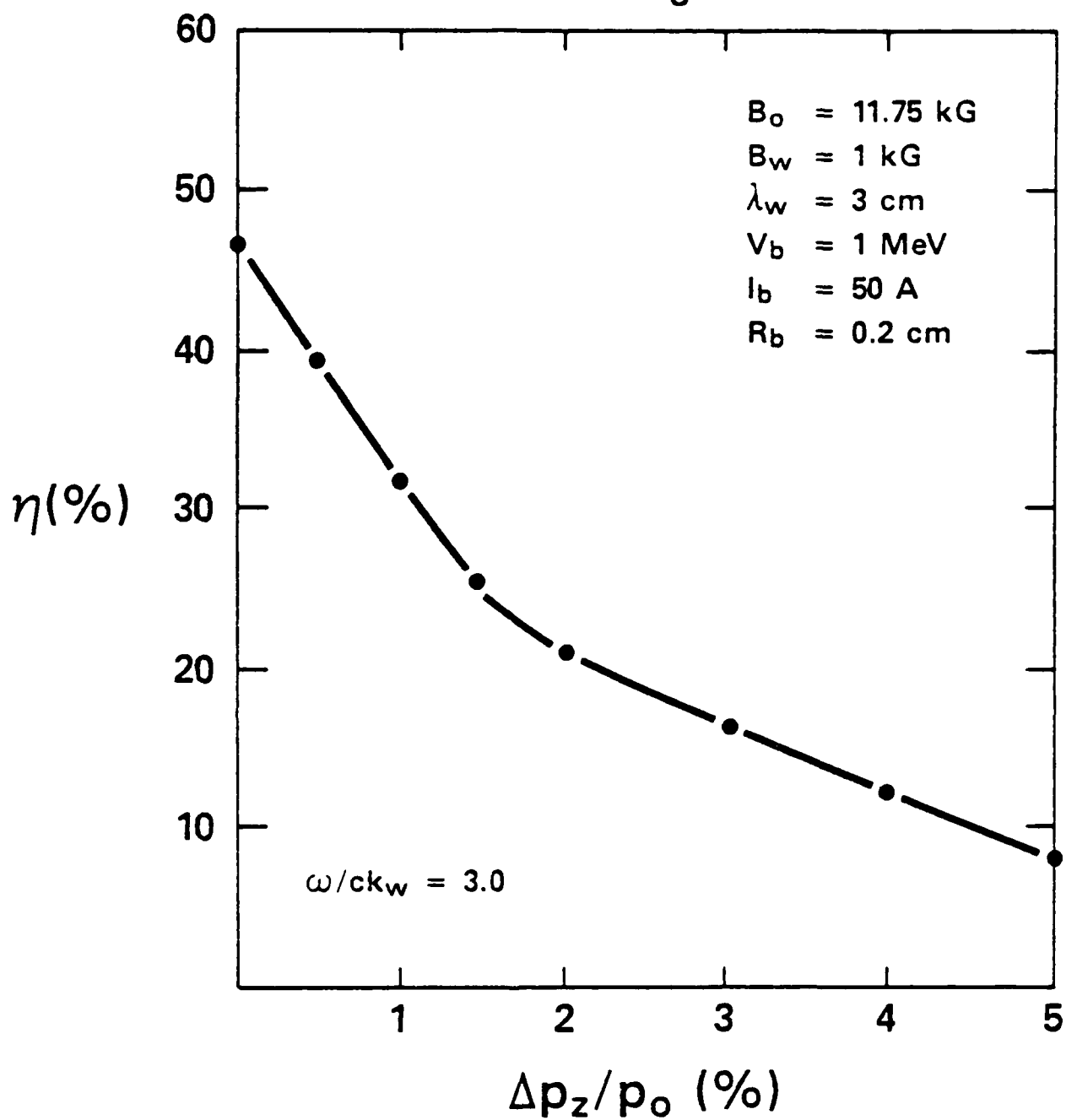


Fig. 4 — Graph of the efficiency versus axial momentum spread for Case 4

END

11-86

DTIC